nature neuroscience

Spontaneous cortical activity alternates between motifs defined by regional axonal projections

Majid H Mohajerani[1,2,6,7], Allen W Chan[1–3,7], Mostafa Mohsenvand[1,2], Jeffrey LeDue[1,2], Rui Liu[1], David A McVea[1,2], Jamie D Boyd[1,2], Yu Tian Wang[2,3], Mark Reimers[4] & Timothy H Murphy[1,2,5]

Using millisecond-timescale voltage-sensitive dye imaging in lightly anesthetized or awake adult mice, we show that a palette of sensory-evoked and hemisphere-wide activity motifs are represented in spontaneous activity. These motifs can reflect multiple modes of sensory processing, including vision, audition and touch. We found similar cortical networks with direct cortical activation using channelrhodopsin-2. Regional analysis of activity spread indicated modality-specific sources, such as primary sensory areas, a common posterior-medial cortical sink where sensory activity was extinguished within the parietal association area and a secondary anterior medial sink within the cingulate and secondary motor cortices for visual stimuli. Correlation analysis between functional circuits and intracortical axonal projections indicated a common framework corresponding to long-range monosynaptic connections between cortical regions. Maps of intracortical monosynaptic structural connections predicted hemisphere-wide patterns of spontaneous and sensory-evoked depolarization. We suggest that an intracortical monosynaptic connectome shapes the ebb and flow of spontaneous cortical activity.

Brain activity related to planned motor output or sensory information exists on a background of spontaneous activity[1,2]. This activity shapes behavior during both sensory and motor tasks, but its purpose and composition are unclear[3]. Spontaneous activity within the anesthetized cat visual cortex[4] can correspond to functional orientation maps[5]. Although the relationship between spontaneous and evoked activity has been explored within a single sensory modality[5–9], what constrains their behavior within larger cortical circuits is less clear. Recurrent patterns of low-frequency (<0.1 Hz) spontaneous activity within larger cortical circuits have been described in rodents, nonhuman primates and human subjects using functional magnetic resonance imaging (fMRI)[10–12] and magnetoencephalography[13,14]. Measurements of both spontaneous and sensory-evoked patterns of fMRI signals have been correlated with fiber tracts between brain sulci[10]. Although imaging of fiber tracts has defined major connections, diffusion tensor imaging cannot distinguish unmyelinated fibers or orientation[15], and fMRI has low temporal resolution[1].

We exploited spontaneous cortical activity to provide a continuous sample of active cortical networks that we assessed using voltage-sensitive dye (VSD) imaging. Unlike fMRI and intrinsic optical signal imaging[16,17], VSD imaging measures electrical activity with relatively high spatial and temporal resolution[18]. VSD imaging has previously been applied across large regions of the mouse cortex to reveal fast, complex, localized and bilaterally synchronized patterns of depolarization[19]. We examined the extent to which patterns of intracortical spontaneous activity reflect the circuits used during sensory processing and their relation to fine cortical structure. To assess the relationship of spontaneous activation patterns to cortical projections, we used a recently available database from the Allen Institute for Brain Science[20]. Analysis of spontaneous activity is advantageous because active arbitrary cortical points can be compared to axonal projections that emanate from the same locations. This strategy works well for areas that cannot be stimulated selectively by sensation but are nonetheless an active part of spontaneous activity, such as the motor cortex, associational areas or the secondary sensory cortex. We show that spontaneous activity within the naive mouse cortex alternates through patterns of activity that can reflect different sensory modalities (somatosensory, visual or auditory) and that are predicted largely by the underlying consensus corticocortical monosynaptic axonal projections.

RESULTS

VSD imaging of activity in anesthetized mouse cortex

Using a preparation with a large craniotomy that exposed the right hemisphere (**Fig. 1a**), we studied interactions between cortical areas using VSD imaging[18]. When stimulating the hindlimbs, forelimbs, whiskers and visual or auditory systems of lightly anesthetized mice, we observed unique regional patterns of cortical depolarization (**Fig. 1b** and **Supplementary Video 1**). All modes of sensory stimulation tested resulted in the initial discrete activation of their primary sensory cortical representation, which was then followed by a nonuniform expansion of depolarization and activation of the posterior and midline cortical areas (**Fig. 1b**, **Supplementary Fig. 1**

[1]Department of Psychiatry, University of British Columbia, Vancouver, British Columbia, Canada. [2]Brain Research Centre, University of British Columbia, Vancouver, British Columbia, Canada. [3]Department of Medicine and Vancouver Coastal Health Research Institute, University of British Columbia, Vancouver, British Columbia, Canada. [4]Department of Psychiatry, Virginia Commonwealth University, Richmond, Virginia, USA. [5]Department of Cellular and Physiological Sciences, University of British Columbia, Vancouver, British Columbia, Canada. [6]Present address: Department of Neuroscience, University of Lethbridge, Lethbridge, Alberta, Canada. [7]These authors contributed equally to this work. Correspondence should be addressed to T.H.M. (thmurphy@mail.ubc.ca).

Received 22 March; accepted 17 July; published online 25 August 2013; doi:10.1038/nn.3499

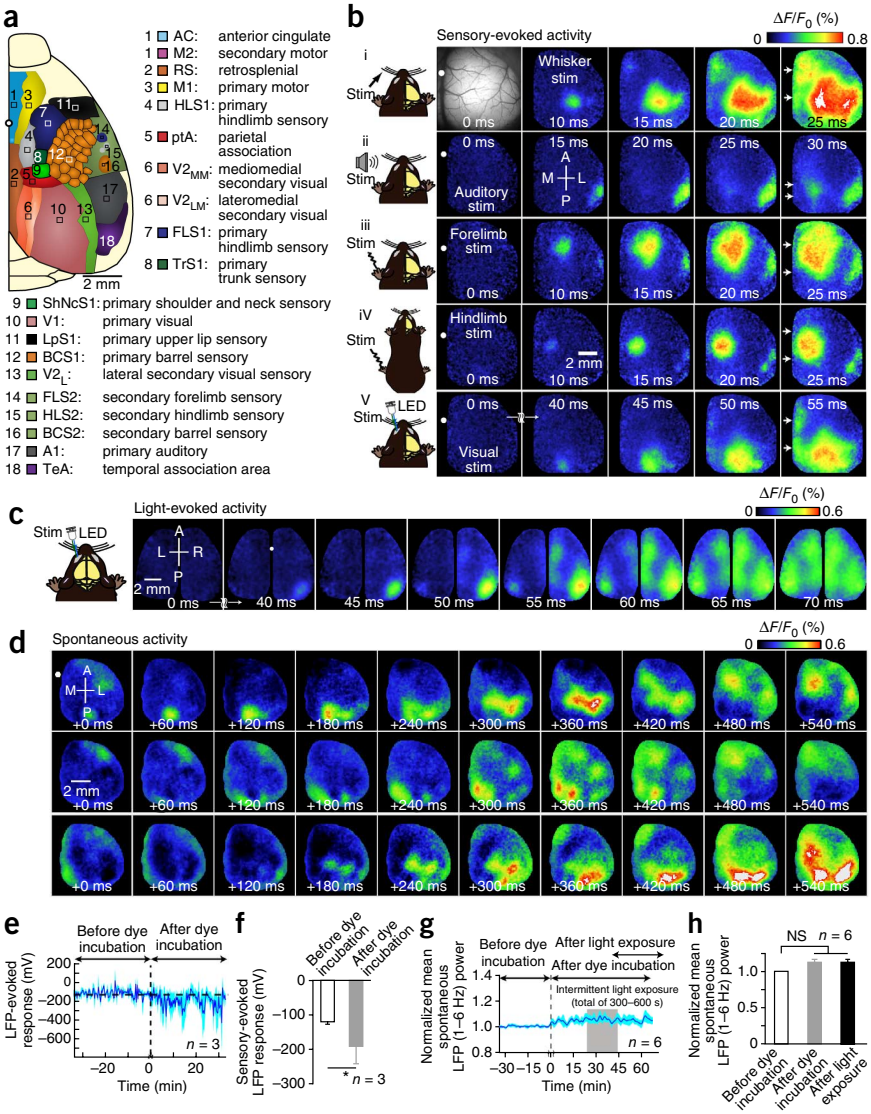

Figure 1 Unique and consensus activation patterns during multiple forms of sensory stimulation. (**a**) Schematic of the unilateral craniotomy showing the imaged cortical regions. (**b**) Photomicrograph of the wide unilateral craniotomy with bregma indicated by a white circle in each image. Patterns of cortical activation are shown in a mouse anesthetized with isoflurane (0.5%) after (i) stimulation (stim) of the contralateral C2 whisker, (ii) auditory stimulation, (iii) contralateral forelimb stimulation, (iv) contralateral hindlimb stimulation and (v) visual stimulation of the contralateral eye with a light-emitting diode (LED). There was midline activation after all forms of sensory stimulation (white arrows) at 10–25 ms after primary sensory cortex activation. The responses are the mean of 20 trials. The image second from the left in the second row indicates the anterior (A), posterior (P), medial (M) and lateral (L) directions. (**c**) Representative montage of VSD responses after visual stimulation of left eye in a bilateral craniotomy. Responses are the mean of ten trials. (**d**) Three independent sequences of spontaneous cortical activity in an anesthetized mouse. Group data analyses are shown in **Supplementary Figures 1** and **4**. (**e**) Time course of the amplitude of repeated (0.05 Hz) forelimb sensory stimulation–evoked responses measured from an LFP electrode placed within FLS1 before and after RH-1692 dye loading. (**f**) Summary of the mean peak amplitudes in **e**. $^*P < 0.05$, one-way ANOVA. Error bars, s.e.m. (**g**) Time course of normalized mean spontaneous LFP power. Recording was resumed 30 min after RH-1692 washout to encompass periods before, during and after intermittent VSD excitation (denoted as light exposure; total illumination time 300–600 s). (**h**) Summary of the LFP power in **g**. Error bars, s.e.m. NS, not significant.

and **Supplementary Video 1**). The activity spread involved the recruitment of secondary, noncontiguous areas of the cortex. Consistent with previous studies of the barrel cortex, we found that brief tactile stimulation of the C2 whisker activated primary somatosensory areas as well as 'islands' of response within functionally related areas such as the primary motor cortex (M1)[6,21–23] and the secondary representation of the somatosensory cortex (S2) (**Fig. 1b**)[22]. Auditory stimulation resulted in activation of the primary auditory cortex (A1) and secondary activation of the cortex centered on the parietal association area (ptA) (**Fig. 1b**). Stimulation of forelimbs and hindlimbs resulted in activation of their respective primary somatosensory areas (FLS1 and HLS1) and recruitment of the respective secondary somatosensory cortices (FLS2 and HLS2) (**Fig. 1b**). Visual stimulation activated the primary cortex (V1), which then spread to the secondary visual cortex (V2) and also recruited midline cortical areas, including the anterior cingulate/secondary motor cortex (AC/M2) and the retrosplenial cortex (RS) (**Fig. 1b**). We observed activation of V1 and associated midline areas within the opposite hemisphere (ipsilateral hemisphere) at around 50 ms after contralateral visual stimulation (**Fig. 1c**). Notably, we observed patterns of spontaneous activity that resembled those present during sensory stimulation (**Fig. 1d** and **Supplementary Video 2**).

Consistent with recent findings[24], incubation with RH-1692 (a VSD) increased the local field potential (LFP) response to sensory stimulation (**Fig. 1e**,**f**); this effect did not seem to be due to general disinhibition, as spontaneous activity assessed by LFP or electroencephalography (EEG) was not affected (**Fig. 1g**,**h** and **Supplementary Fig. 2c**,**d**). In addition, the magnitudes of the RH-1692–facilitated sensory-evoked responses fall within the range of excitability changes observed resulting from anesthesia on the amplitudes of sensory-evoked responses (**Supplementary Fig. 2f**). We include RH-1692 facilitation of excitability as a potential caveat of these studies but argue that in the absence of an experimental model of widespread cortical expression of voltage-sensitive fluorescent protein[25], it may be the best available means of imaging of widespread cortical activity.

We quantified the sensory-evoked spread of VSD activation using a combined local-global method of optical flow measurement[26]. A similar approach has been used previously to quantify VSD cortical dynamics[27]. We determined the direction and velocity of cortical depolarization for each image after stimulation (**Fig. 2a** and **Supplementary Video 3**). We derived maximum velocity measurements (**Fig. 2a** and **Supplementary Video 3**) for patterns of activity induced for each mode of stimulation. We then plotted the movement of the maximum velocity position during activity spread over the

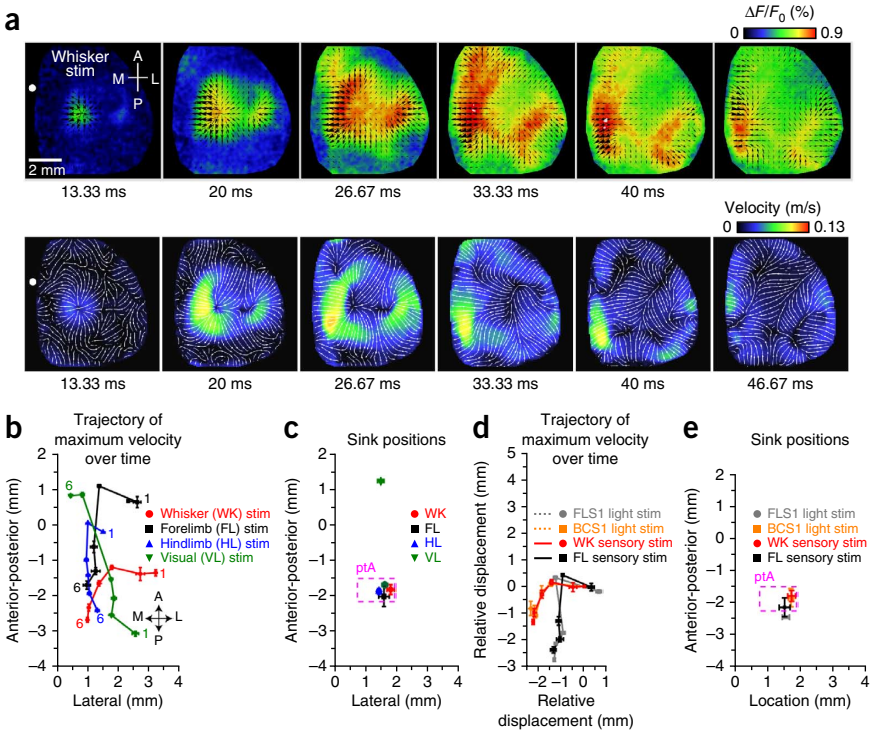

Figure 2 Sensory- and photostimulation-induced activation show modality-specific source locations and termination at a common sink location. (**a**) Top, whisker stimulation–evoked VSD activation (average of 20 trials). Black arrows indicate the direction of velocity of the VSD signal spread, and the relative magnitudes of velocity are indicated by the size of the arrows. Bottom, measurements of the absolute velocity of the responses in the top row are represented in pseudocolor. Streamlines indicate the local direction of velocity flow. (**b**) Position of maximum velocity (center of mass) of the VSD signal spread resulting from sensory stimulation after the initial activation of the cortex relative to the bregma during six 6.67-ms intervals, labeled 1–6. The bregma is at coordinate (0,0). Error bars, s.e.m. (**c**) Positions of sink locations for each sensory modality plotted on the cortex relative to the bregma. All forms of sensory stimulation shared a common sink location within ptA, indicated by a dotted box ($P > 0.05$, $n = 8$ mice). Visual stimulation resulted in an additional sink location within the anterior medial cortex ($P < 0.001$ for comparisons to the distribution simulated under the null hypothesis, $n = 8$ mice). Error bars, s.e.m. (**d**) Positions of the maximum velocity of VSD signal spread after sensory stimulation (forelimb and whisker) and photostimulation (FLS1 and BCS1). The maximum velocity positions for each trajectory were normalized to their initial positions. The trajectories from sensory stimulation and photostimulation were similar ($P > 0.05$ for sensory stimulation compared to photostimulation of the same of modalities, $n = 7$ mice). Error bars, s.e.m. (**e**) Positions of sink locations for sensory- and photostimulation-induced activation plotted on the cortex relative to the bregma. The sink locations between sensory-evoked and photostimulation-induced activation were similar ($P > 0.05$ for all comparisons, $n = 7$ mice). Error bars, s.e.m.

cortex (**Fig. 2b**), which indicated stimulus-specific source locations at the associated primary sensory cortices that was followed by movement of the responses toward more medial areas (**Fig. 2b**). Although the source locations were stimulus specific, there was a common sink location within ptA for activity induced by sensory stimulation (**Fig. 2c**). Visual stimulation showed a second more anterior sink location near AC/M2 (**Fig. 2c**).

To assess whether the spread of activation was derived from consensus intracortical circuits (that were independent of sensory processing), we repeated the optical flow analysis for intracortical activity stimulated by channelrhodopsin-2 (ChR2) within Thy-1 transgenic mice[22]. The characteristics of the activity spread were similar with respect to whether the spread was induced by sensory stimulation (whisker or forelimb) or by direct ChR2-mediated activation of the associated primary sensory cortices (the primary representation of the barrel cortex (BCS1) or FLS1) (**Fig. 2d**). Consistent with this observation, the sink locations for activity spread resulting from sensory stimulation or photostimulation of the cortex were also similar (**Fig. 2e**).

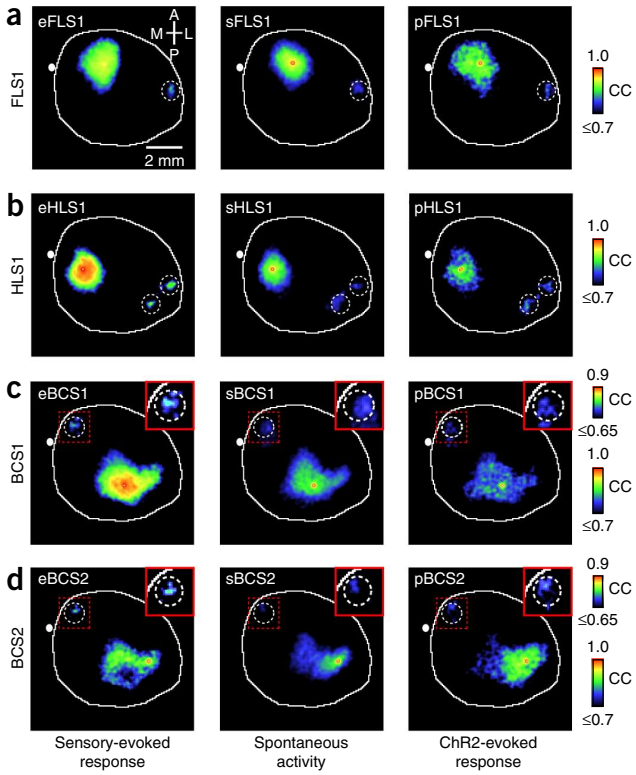

Figure 3 Spontaneous, sensory- and photostimulation-evoked cortical VSD maps share similar regional patterns. (**a**) Representative correlation maps from a seed pixel located within the primary representation of FLS1 generated from VSD signals after sensory stimulation of the contralateral forelimb (eFLS1; left), during 300 s of cortical spontaneous activity (sFLS1; center) or after direct photostimulation of FLS1 (pFLS1; right). There was a distant correlation at FLS2, as indicated by white dashed circle. CC, correlation coefficients (color coded). (**b**–**d**) Similar to **a** but locating the seed pixel within HLS1 (**b**), BCS1 (**c**) or the secondary representation of the C2 barrel cortex (BCS2; **d**). Distant areas of high correlation are highlighted by white dashed circles. The inset images show magnifications of the areas in the dotted red boxes, and correlation coefficient values were all rescaled to the calibration bars on the right. Group data analyses are shown in **Supplementary Figures 3** and **5**.

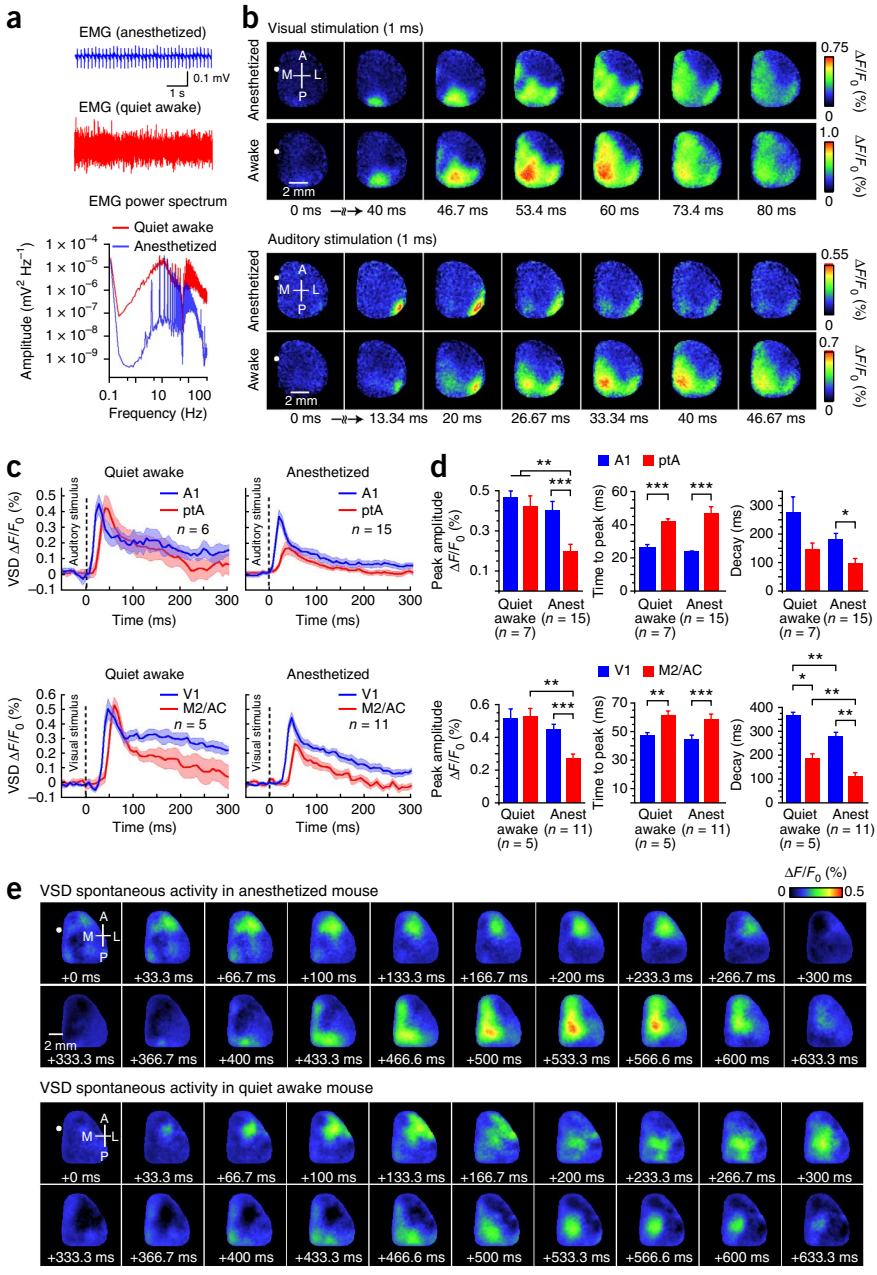

Figure 4 Patterns of sensory-evoked and spontaneous activity in quiet awake mice are similar to those observed under anesthesia. (**a**) Individual example of neck muscle EMG (>1 Hz) from a head-restrained mouse under isoflurane (0.5%) anesthesia (top trace) or 1 h after awakening (bottom trace). The power spectra of the EMG signals are different between states of anesthesia (blue) and wakefulness (red). (**b**) Representative cortical VSD signals in response to contralateral visual or auditory stimulation during anesthesia or in quiet awake states. The images represent the average of ten trials of stimulation. The responses are scaled differently. (**c**) Quantification of the VSD signals in response to auditory or visual stimulation in anesthetized or quiet awake states. Plots are the average of the VSD signals measured from 5 × 5 pixel boxes (~0.11 mm^2) placed within A1 (blue traces) and ptA (red traces) for auditory stimulation or within V1 (blue traces) and M2/AC (red traces) for visual stimulation. The thickness of the shading around each plot indicates the s.e.m. (**d**) Statistical quantification of peak amplitude, time to peak and decay of auditory-evoked and visual-evoked VSD responses during anesthesia or the quiet awake state. Error bars, s.e.m. $^{**}P < 0.01$, $^{***}P < 0.001$, one-way ANOVA. (**e**) Representative montages showing two distinct time periods (633.3 ms each) of VSD imaging of spontaneous cortical activity during anesthesia or in a quiet awake state.

Diverse activity sources create similar correlation maps

In anesthetized mice, spontaneous cortical activity is dominated by slow-wave activity with greatly reduced power at higher-frequency bands[19] (**Supplementary Fig. 2**). By examining sequences of slow-wave spontaneous cortical activity (0.1–6 Hz) using VSD imaging in anesthetized mice, we observed regional patterns that at times resembled those present in the averaged trials of sensory stimulation (**Fig. 1d** and **Supplementary Video 2**). Spontaneous slow-wave activity has been recorded in the absence of external stimulation to sensory systems using equipment that did not produce discernible vibration or auditory stimulation[19]. As in that study, the red light used to excite VSD fluorescence was directed away from the eyes and was applied continuously to avoid intermittent stimulation[19]. To analyze patterns of spontaneous activity quantitatively, we made correlation maps based on a seed pixel within the center of a distinct cortical area (Online Methods), which is similar to the methods used in a previous seed-voxel correlation analysis in resting-state fMRI data to detect functional connectivity[28]. Using a seed pixel within FLS1 in an anesthetized mouse, we examined its correlation to all other pixels within the imaged cortex during a 300-s period (6.7-ms frames, 0.1–6 Hz) of spontaneous activity (sFLS1; **Fig. 3a**). **Supplementary Video 4** shows the cumulative seed pixel–based correlation maps for the forelimb cortex alongside the spontaneous activity used to create them. The correlation values in the map are highest around the seed pixel and include areas that are functionally related over the period chosen to measure spontaneous activity. Comparison of these spontaneous or sensory-evoked correlation maps using spatial correlation analysis indicated similarity (**Supplementary Figs. 3** and **4**). With respect to the hindlimb cortex, correlation maps generated from time series of spontaneous activity with seed pixels within the hindlimb cortex (sHLS1) were similar to the correlation map generated from hindlimb sensory-evoked activity (eHLS1) (**Fig. 3b** and **Supplementary Figs. 3** and **4**). We used similar approaches to compare correlation maps obtained from spontaneous and evoked activity within other sensory modalities, such as audition (**Supplementary Figs. 4e** and **5a**), vision (**Supplementary Fig. 4f**) and vibrissa sensation (**Fig. 3c** and **Supplementary Figs. 3** and **4b**), or regions that were not selectively accessible by peripheral sensory stimulation, such as the secondary representations of sensory cortices (**Fig. 3d** and **Supplementary Fig. 5a**). To control for the contribution of correlation coefficient values near the seed-pixel location, we subtracted these values before

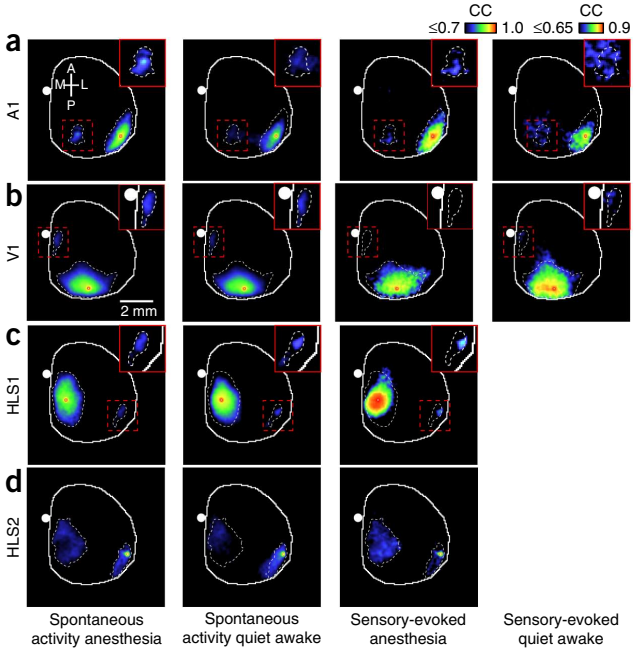

Figure 5 The correlation maps generated from sensory-evoked or spontaneous activity during quiet wakefulness are similar to the maps obtained during anesthesia. (**a**) Representative correlation maps generated from a seed pixel from A1 calculated from 300 s of cortical spontaneous activity in isoflurane-induced anesthesia (left), quiet wakefulness (middle left) or after auditory stimulation in an anesthetized (middle right) or quiet awake (right) state. White dash outlines represent highlighted areas of correlation obtained from spontaneous activity under anesthesia. The inset images show magnifications of the areas in the dashed red boxes in which the correlation coefficient values were all rescaled to the calibration bars above the inset on the right. (**b**–**d**) Similar to **a**, but the correlation maps were calculated within V1 (**b**), HLS1 (**c**) or HLS2 (**d**). Group data analyses are shown in **Supplementary Figure 7**.

performing spatial correlation analysis (Online Methods). In this manner, we excluded local functional connections and focused on second-order, distant connections exclusively. In all cases, there was strong correspondence between the correlation maps of spontaneous and sensory-evoked activity belonging to the same cortical location (**Supplementary Fig. 3b**).

We repeated the seed-pixel correlation analysis for intracortical evoked activity stimulated by ChR2 (ref. 22) to assess whether these correlations were derived from consensus intracortical circuits that were independent of sensory processing. Optogenetic stimulation of a cortical area resulted in patterns that closely resembled those from spontaneous activity involving that area or those from sensory stimulation (**Fig. 3**). Seed-pixel correlation maps generated from VSD imaging of spontaneous, sensory-evoked or photostimulation-evoked cortical activity indicated similarity between the three types of maps (**Supplementary Fig. 3b**). This is consistent with the similarity we observed using region of interest (ROI)-based correlation analysis (**Supplementary Fig. 4**). In contrast, when we compared

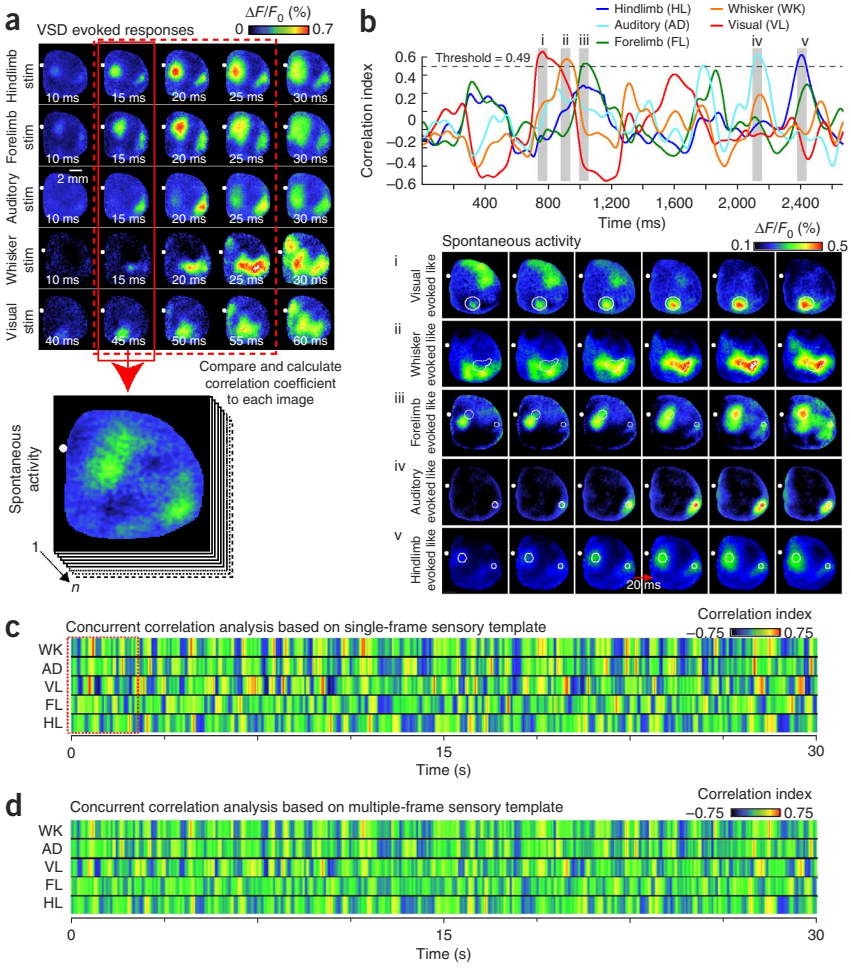

Figure 6 Spontaneous cortical activity can be decomposed into unique repeating sensory motifs. (**a**) Representative montages show examples of the VSD response to five different forms of sensory stimulation. Each image of spontaneous activity was compared with the sensory-evoked templates (the pattern at the initial cortical response, highlighted by the solid red box). VSD responses represent the average of 20–45 trials of stimulation. (**b**) Top, plot of the concurrent correlation of instantaneous patterns of spontaneous activity (2.6 s of spontaneous VSD data) with multiple templates of sensory-evoked responses. Spontaneous activity was considered to be a 'match' to the evoked template if the correlation value was greater than a given threshold (**Supplementary Fig. 8a**). Bottom, representative montages (20-ms intervals) showing cortical spontaneous activity that resembles sensory stimulation–derived templates, corresponding to the shaded gray regions highlighted in the graph above. White outlines represent areas of activation that were associated with the sensory stimulation–derived template. (**c**) Pseudocolor image representing a 30-s time course of the concurrent correlation of different templates of sensory-evoked responses with a 30-s period of spontaneous activity. The red dashed square outlines the first 2.6 s of spontaneous VSD data (corresponding to the top plot in **b**). The color of each column of pixels represents the correlation value at the different times. (**d**) Concurrent correlation as in **c** but using templates of sensory-evoked responses containing the first three frames of sensory-evoked activity after the initial response (highlighted by the dashed red box in **a**).

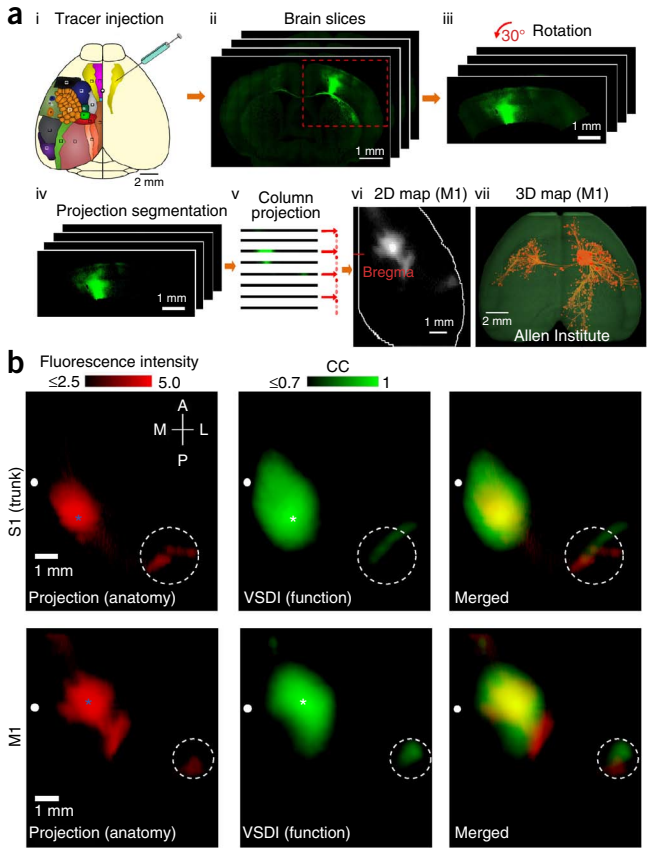

Figure 7 Comparison of cortical axonal projection patterns to correlation maps of spontaneous cortical activity. (**a**) (i) Schematic showing injection of the AAV tracer to map axonal projections of different cortical regions within the adult mouse brain (data obtained from the Allen Institute for Brain Science). The color-coded cortical locations are as described in **Figure 1a**. To quantitatively compare the axonal projection maps with the functional correlation maps, two-dimensional (2D) representations of AMBC Atlas data sets were created (ii–vi; Online Methods). (vii) Three-dimensional (3D) reconstruction, produced using the Brain Explorer software from the Allen Institute for Brain Science, of M1 axonal projections (image credit, Allen Institute for Brain Science). (**b**) Left, examples of S1 trunk and M1 axonal projection maps. The pixel intensities are scaled logarithmically. Center, seed-pixel correlation maps obtained from VSD imaging of spontaneous activity within S1 trunk or M1. Right, spatial colocalization of axonal projection (left) and correlation (center) maps. White dashed circles indicate the position of S2. Blue and white stars indicate the positions of the tracer injection and the seed pixel, respectively. See **Figure 8** for group data analysis.

maps across different sensory cortices, we found significant differences ($P < 0.001$ for all BCS1 and LPS1 comparisons, $P < 0.05$ for all other comparisons, one-way analysis of variance (ANOVA); **Supplementary Fig. 3b**). Correlation maps were not produced after application of 30 μM tetrodotoxin (TTX) to the cortex, indicating a dependence on neuronal activity and that correlation due to other factors is low (**Supplementary Fig. 5c**,**d**). Shuffling of pixel values within each frame of imaged cortex before seed-pixel correlation analysis did not produce these maps (**Supplementary Fig. 5e**,**f**). Distinct correlation maps of both spontaneous and sensory-evoked activity were apparent even when we examined neighboring cortical regions at a distance of only 0.5 mm, providing a minimum estimate of VSD spatial resolution (**Supplementary Fig. 5a**,**b**).

VSD imaging of cortical activity in quiet awake mice

The results in **Figures 1–3** and **Supplementary Figures 1–6** were obtained from mice under isoflurane anesthesia to reduce movement artifacts or activity related to voluntary behavior. In awake rodents engaged in specific tasks such as whisking, cortical spontaneous activity is desynchronized[3,29], and the cortical responses show enhanced synaptic inhibition[30]. In contrast, cortical neurons of quiet awake rodents show oscillations that are synchronized both locally[8,29] and across hemispheres[19]. We examined whether sensory stimulation or spontaneous activity in quiet awake mice evoked similar, stereotypical patterns of activity as those observed in anesthetized mice. We imaged both spontaneous and sensory-evoked cortical activity in head-fixed, awake mice and also in mice that were subsequently anesthetized with isoflurane. Using a second camera to monitor the movements of the mice (mainly the forepaws and whiskers) and an electromyography (EMG) electrode inserted in the neck to measure muscle tone, we classified the state of the mice as either anesthetized or quiet wakefulness (**Fig. 4a** and **Supplementary Fig. 2e**). Under these conditions, we recorded the spatiotemporal dynamics of activity in response to sensory stimulation (visual or auditory) and during spontaneous activity under conditions of isoflurane anesthesia or in a quiet awake state (**Fig. 4b–e**). Quantification of sensory-evoked VSD response parameters, such as peak amplitude and time to peak, in the anesthetized and quiet awake states measured from the center of V1 or A1 did not show significant differences (**Fig. 4b–d**). In both the anesthetized and quiet awake states, we observed activation of distant areas such as ptA and M2/CG for auditory and visual stimulation, respectively (**Fig. 4b–d** and **Supplementary Video 5**).

Region-specific intracortical seed-pixel correlation maps generated from spontaneous or sensory-evoked activity were similar in anesthetized and quiet awake mice (**Fig. 5** and **Supplementary Fig. 3c**). These data suggest that functional connectivity can be inferred from data using light isoflurane anesthesia.

Reverberation of sensory motifs in spontaneous activity

To characterize the distribution of spontaneous activity motif repeats over time, we used a whole-frame spatial correlation approach in which we compared sequences of spontaneous activity to templates that reflect the onset of cortical activation[5] created from average VSD activity patterns evoked by multiple modes of sensation (**Fig. 6a** and Online Methods). This analysis yielded a single correlation value for the comparison of each image frame of spontaneous activity with an image template (**Fig. 6b**). Hindlimb-, forelimb-, auditory-, whisker- and visual-stimulation templates were correlated to 30 s of spontaneous activity in isoflurane-anesthetized mice, yielding plots of correlation coefficients versus time (**Fig. 6b**,**c**). Within these time plots, we observed peaks at which selected sequences of spontaneous activity closely resembled the sensory template images (**Fig. 6b**). We found that these cortical activity motifs within spontaneous activity repeated when we examined prolonged sequences of spontaneous activity (**Fig. 6c**). At times, spontaneous activity resembled a single sensory modality response exclusively, whereas at other times, overlap was apparent between multiple sensory modalities. Repeats of cortical activity motifs were apparent at much lower rates when motifs derived from randomly placed blobs that resembled cortical activity were used as templates (**Supplementary Fig. 6b–d**). In addition, sensory motifs were not present in the spatially shuffled data (**Supplementary Fig. 6e**,**f**).

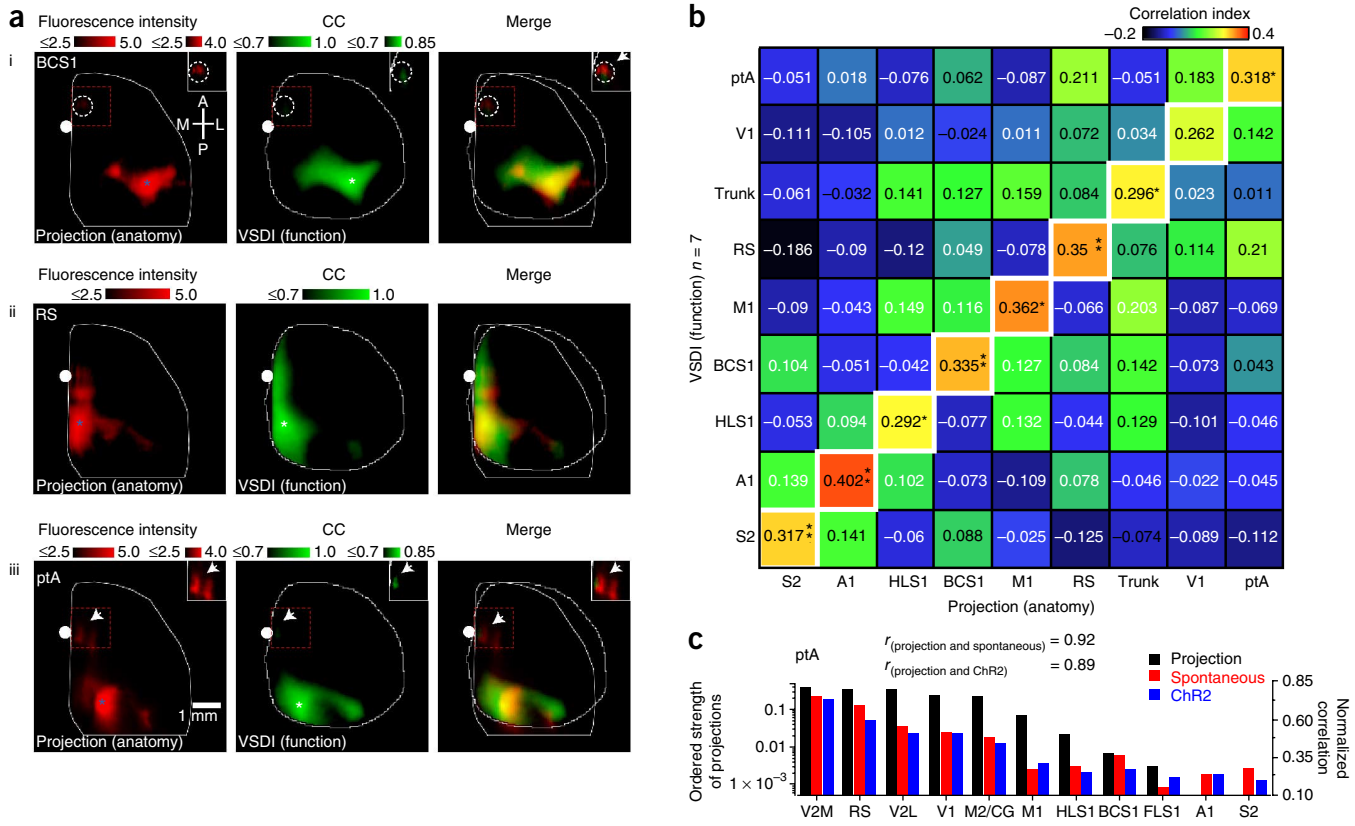

Figure 8 Axonal projection maps are most similar to their corresponding functional maps. (**a**) (i) Axonal projection maps (left) of BCS1. The blue asterisk denotes the AAV injection site. The pixel intensities are scaled logarithmically. There is relatively weak pixel intensity in the area outside the injection site (dashed circle). Seed-pixel correlation map (center; with a presumed similar location to the AAV injection site) of BCS1 obtained from spontaneous activity. The white asterisk denotes the location of the seed pixel. Right, overlay of the anatomical and correlation maps. White solid outlines indicate the boundary of the imaged cortex. Inset images are magnifications of the areas in the dashed red boxes and were all rescaled to the color calibration bars above the insets on the right. (ii,iii) Similar to i, axonal projection and correlation maps are shown for RS (ii) and ptA (iii). (**b**) Matrix showing similarity between VSD correlation ($n = 7$ mice) and axonal projection maps for nine cortical regions. $^{*}P < 0.05$, $^{**}P < 0.01$, one-way ANOVA. (**c**) Ordered strength of ptA axonal projections (black) to 11 ROIs compared to normalized correlation maps obtained from spontaneous activity (red; $n = 10$ mice) or ChR2-evoked VSD responses (blue; $n = 6$ mice). ROIs are ordered based on strength of ptA axonal projection density to other ROIs. The rank order of axonal projection strength was similar to the rank order of functional connectivity strength measured from both spontaneous activity and ChR2-evoked responses ($P < 0.001$ for both comparisons, Spearman's rank correlation). Tests of significance were made against a null hypothesis of axonal projection strength and HLS1 functional connectivity strength ($r_{\text{projection(ptA) and spontaneous(HLS1)}} = -0.37$, $r_{\text{projection(ptA) and ChR2(HLS1)}} = -0.38$, $P > 0.20$ for both comparisons).

To estimate the fraction of variance associated with cortical sensory motifs, we used a regression approach with five separate sensory motifs and found that these motifs accounted for 18.5 ± 1.1% (mean ± s.e.m.) of total the VSD signal variance of spontaneous activity (0.1–6 Hz bandpass filtered, $n = 7$ mice). Given that there are probably more than five sensory motifs, and probably also many for nonsensory activity, this represents a lower limit. As a further test of repeating motifs within spontaneous activity, we used a sensory template composed of the first three frames after the initial VSD response and found general agreement with the results obtained from a single image, but the peak correlations were blunted (**Fig. 6d** and **Supplementary Videos 6** and **7**). Three frame templates were able to recover modality-specific patterns from spontaneous activity that resembled sensory responses but at a slower timescale (**Supplementary Fig. 1c** and **Supplementary Videos 6** and **7**).

Cortical axonal projections and functional connectivity

To assess how the regional patterns of VSD response related to the underlying structural circuits, we examined the Allen Mouse Brain Connectivity (AMBC) Atlas. This atlas provides axonal projections that are labeled with the anterograde tracer GFP expressed using adeno-associated virus (AAV) injection into discrete cortical locations and brain nuclei of C57BL/6 mice[20]. These mice were the same strain and age range of the mice that we used in our study. We chose to make comparisons between spontaneous activity patterns and axonal projections, as the seed-pixel correlation method allowed us to determine the regional functional connectivity associated with the same sites that were targeted in the AMBC Atlas for injection of AAVs. Although both axons and dendrites were labeled with GFP, we quantified projections >0.5 mm from the AAV injection-site center, which were mostly long-range axonal projections. We processed the three-dimensional structural data to match the perspective of our two-dimensional VSD images (**Fig. 7a**).

By examining axonal projections in the two-dimensional flattened representations in the AMBC Atlas that emanated from the primary trunk cortex and comparing these to the correlation map of spontaneous VSD activity for the same region measured in anesthetized mice, we observed strong spatial colocalization (**Fig. 7b**). Furthermore, we observed similar colocalization within M1 (**Fig. 7b**) and other regions examined (**Fig. 8a** and **Supplementary Fig. 7c–f**). Maps of

axonal projections and VSD activity correlation maps were colocalized (on the basis of spontaneous cortical activity) for injections that targeted the same cortical area within different mice (**Supplementary Fig. 7a**,**b**). As some local correlation between structure and function would be apparent because of local spread of AAV labeling around the injection site, we removed the area centered over the injection or seed pixel used in the correlation analysis of functional data using a Gaussian fit and subtraction procedure in our statistical comparisons (**Supplementary Fig. 8**). We examined local correlation attributed to nonbiological sources such as image sampling and estimated the point-spread function to be <67 μm (1 pixel). We compared the spatial correlation of axonal projections for nine cortical areas with the corresponding functional correlation maps determined by VSD imaging (**Fig. 8b**; $n = 7$) and observed that the axonal projection structure was related to cortical function, as assessed using VSD imaging. It should be noted that although the VSD correlation maps for ptA were the most similar to the structural map of the ptA axonal projection, the RS map for structural connectivity also showed a high value of correlation, as the axons within these two regions overlap (**Fig. 8a**,**b** and **Supplementary Fig. 7c**,**f**). As an alternative means of comparing structural and functional cortical connectivity, we used an ROI-based analysis. When we compared the strength of the parietal-association cortex axonal projections to 11 ROIs of functional correlation maps measured using VSD imaging of spontaneous activity or seed-pixel correlation analysis of photostimulation-evoked responses (**Fig. 8c** and **Supplementary Fig. 9** for additional cortical regions), we found evidence that a significant ($r_{\text{projection(ptA) and spontaneous(ptA)}} = 0.92$, $r_{\text{projection (ptA) and ChR2(ptA)}} = 0.89$, $P < 0.001$ for both comparisons; tests of significance were made against a null hypothesis of axonal projection strength and HLS1 functional connectivity strength using Spearman's rank correlation) amount of the VSD cortical dynamics were explained by underlying patterns of monosynaptic axonal projections.

When we differentiated the axonal projection maps of labeled neurons within different injection locations into the supragranular layers I–III as compared to infragranular layers V–VI, we found that the axonal projection maps were similar across the cortical laminae (**Supplementary Fig. 10**). It is therefore plausible to use VSD imaging that detects mainly superficial cortical activity[18] for comparison to maps extracted from axonal tracing results from all layers.

DISCUSSION

VSD imaging of cortical activation motifs

We used VSD imaging to monitor cortical activity over rapid physiologically relevant timescales[5,6,9,18,19,22,31,32]. This approach permits the comparison of these functional networks to the underlying axonal monosynaptic projection structure[20]. We demonstrated the unique regional cortical motifs that are associated with different forms of sensory stimulation and the ability of spontaneous activity to contain representations of these widespread circuits. We observed that sensory-induced, photostimulation-induced or spontaneous activation leads to intracortical spread of the VSD depolarizing response. This result may seem to be at odds with the idea that sensory activation should be relatively restricted and limited primarily to somatotopic areas[33]. However, VSD imaging can detect both subthreshold and suprathreshold activity[18]. Given the relatively long time course of subthreshold events, their contribution to VSD signals can be substantial and may indicate a modulatory role[16,33].

The observation of extensive intracortical spread of depolarization is consistent with previous intrinsic signal optical imaging combined with electrophysiological recording data from the somatosensory and auditory cortices[16]. Likewise, voltage-sensitive fluorescent protein imaging has revealed a spread of depolarization resulting from sensory stimulation that extends several millimeters[25]. Although depolarizing events can spread over a considerable distance, they nonetheless show specificity. In examining different forms of sensory stimulation, we observed modality-specific cortical activation patterns. For example, visual stimuli lead to V1 activation, and auditory stimuli lead to A1 activation with a relatively short latency. At later times, divergent sensory stimuli lead to common patterns of activation that include ptA and midline activation (M2/AC and RS). The propagation of sensory-evoked activity along these midline routes and frequent activation of these same regions by spontaneous activity[19] suggest that these regions are hubs within the mouse cortex[22] in which multiple forms of sensory information integrate during both evoked and spontaneous cortical activity. The spread of activation to sinks within posterior midline areas such as ptA is consistent with similar areas forming a connectional core within the human brain[1].

State dependence of cortical activity motifs

We report patterns of intracortical spontaneous and sensory-evoked activity for quiet awake and lightly anesthetized mice. The spread of activity from primary activation areas to distant but anatomically and functionally connected regions (for example, the anterior cingulate for visual stimuli and the parietal-association cortex for auditory stimulation) became stronger in the awake state. This awake state–dependent increase of functional connectivity may be essential for the integration of multisensory information and perception[3]. It is probable that subtleties within the cortical state that are associated with different behaviors will modify the regional patterns we observed[3,29]. Ultimately, functional studies will need to be conducted under specific scenarios to examine additional state-dependent connectivity relationships[3,8,19,34]. However, similarity in connectivity patterns between the quiet awake and anesthetized data and their relationship to the core structural connections suggest that major activity patterns under anesthesia will probably translate to different cortical states that are associated with active task engagement[3,10].

Although similar correlation maps were observed between the quiet awake and anesthetized states, recent data indicate that during wakefulness, cortical responses show enhanced synaptic inhibition that may restrict the spatiotemporal structure of the evoked responses[30]. Similarities in the correlation maps for quiet awake and anesthetized activity probably reflect strong consensus intracortical pathways and do not necessarily imply that these two brain states use identical temporal or microscopic circuit features.

Spontaneous activity is a resource of circuit activity

We exploited spontaneous activity to provide a rich palette of cortical activity that can be captured by VSD imaging. Advantages of using this approach include the ability of cortical circuits to be sampled in a repeated manner, even with multiple response patterns occurring concurrently. Furthermore, the analysis of spontaneous activity allowed the simultaneous observation of the functional connectivity of sensory regions as well as arbitrary points that cannot be activated directly by sensory stimulation. The advantage of using spontaneous activity and single pixel–based correlation analysis is that we can derive functional relationships for any site that was targeted by AAV injection for determination of regional axonal projections.

To establish associations between the AMBC Atlas injection sites and the equivalent functional sites, we used functional landmarks for alignment, such as the center of V1 or A1, that are experimentally defined by sensory stimulation and are present within the AMBC Atlas

structural data set, in addition to using anatomical landmarks. There could be errors in positioning, although the use of functional and anatomical landmarks should minimize them. Given the close correspondence between the spontaneous and evoked activity response patterns, we do not anticipate major differences in functional connectivity maps if evoked activity were used instead of spontaneous activity for comparison with anatomical connectivity maps.

Spontaneous activity contains motifs of sensory activity

We demonstrate that repeating circuit motifs used during sensory processing are present in spontaneous activity. This concept may be similar to the recall of patterned activity within memory tasks that has been observed in the hippocampus and prefrontal cortex[35,36]. To identify cortical motifs, we used a single image that reflects the onset time of the sensory responses. Although templates based on multiple images may be more stringent, the eventual flow of activity from the initial selective points to more general cortical sinks degrades specificity. Further analysis of images using independent component analysis[1,28] may be informative for decomposing spontaneous activity into multiple network maps that group correlated regions together.

Although we describe the contribution of sensory motifs to cortical spontaneous activity, it is probable that unique motifs associated with nonsensory activity are also present. We currently have a limited understanding of the activity motifs that are associated with higher cognitive function[1]. We anticipate that these motifs may be defined using specific behavioral assays[1,6] or perhaps optogenetics to directly activate subsets of these circuits[22].

Relation of activity propagation to axonal projections

Records of VSD coactivation are highly correlated with monosynaptic axonal projections. The distances over which we observed intracortical VSD signal propagation are on the order of 0.5–6 mm, which is within the range of monosynaptic intracortical axonal projections[37]. This suggests that the major horizontal architecture of the cortex for relaying information over rapid time scales may predominantly involve single projections. This is consistent with previous work done in the barrel cortex[6,23], which we extended to additional regions of brain and, in particular, associational areas that cannot be studied using sensory stimulation. Although long-range relays are single projections, once this activity arrives at its destination, it is probably distributed to a columnar canonical cortical microcircuit[37,38]. The correlation analysis we performed assumed little or no lag between the different regions of the cortex. We highlight short-latency relationships here, although it is possible that by adding negative or positive time lags to the correlation analysis[39], both upstream and downstream circuits may be studied.

We show similarity between functional connectivity maps obtained from patterns of VSD signals and maps of structural connectivity, although we caution that there is not a linear relationship between projection intensity and the strength of the functional connections determined by VSD activity. For comparison of these quantities, we used a spatial correlation analysis for VSD signals versus linear or log-transformed values of axonal projection intensity. In this case, given the dissimilar quantities being compared, we suggest caution regarding quantitative statements about the relationship between VSD correlation coefficient maps and axonal projection intensity. Instead, we examined the relative spatial distribution of each. Projection maps illustrating long-range axonal connections can sometimes appear discontinuous, with gaps between the source and target areas. The target areas within these maps represent terminal axonal arbors that are connected over long distances through axonal projections that transit the subcortical white matter, which is consistent with findings in anatomical studies. The emergence of ascending axons and their arbors toward superficial layers may contribute to the apparent similarity in the supragranular and infragranular anatomical maps. However, this does not imply that there are not important differences between deep and superficial cortical circuitry but instead suggests that they were not observed at our level of assessment. An alternative model for traveling-wave propagation is through bidirectional cortical-thalamic loops[33,40]. Although most of the VSD response patterns we observed are consistent with underlying cortical structural projections, we cannot exclude a role for cortical-subcortical loops[41].

Our current work compares VSD response patterns to structural projections made using monosynaptic anterograde tracers. Using retrograde polysynaptic rabies virus tracers[42], it would be possible to target multisynaptic pathways. These experiments could also involve rabies viruses that permit both structural and functional analyses using optogenetic tools to manipulate upstream projections[43].

Although we argue that much of the intracortical functional architecture can be described through these apparently monosynaptic excitatory projections, we do not exclude a role for intracortical inhibitory circuits[44] in shaping these signals. However, most inhibitory projections do not span long distances[45]. A more detailed analysis of cortical activity[46] will probably reveal cortical layer–specific functional connections that may be influenced by local intracortical inhibition. We used positive correlation to examine areas that are coactivated. It may also be possible to examine areas that are negatively correlated, where one region may inhibit another[45].

We are fortunate that the AMBC Atlas data set is derived from the same type of C57BL/6 mice that we used in our analyses. Studies of cortical connection structure[47–49] and function could be extended to animals that model disease. Investigators have begun to develop hardware to stimulate circuits that have been lost because of ischemic damage[50]. Brain stimulation may be aided by the knowledge of cortical functional connections, which may lead to rationally designed stimulus paradigms that could be translated to patients using transcranial magnetic stimulations, transcranial direct current or even optogenetics.

METHODS

Methods and any associated references are available in the online version of the paper.

Note: Any Supplementary Information and Source Data files are available in the online version of the paper.

ACKNOWLEDGMENTS

This work was supported by Canadian Institutes of Health Research (CIHR) Operating Grant MOP-12675 (T.H.M.), a Human Frontier Science Program grant (T.H.M.), Michael Smith Foundation for Health Research postdoctoral fellowships (M.H.M. and A.W.C.), a CIHR Operating Grant (Y.T.W.), Heart and Stroke Foundation of Canada postdoctoral fellowships (M.H.M. and A.W.C.) and a CIHR Focus on Stroke postdoctoral fellowship (M.H.M.). We thank the Allen Institute for Brain Science for providing a database of axonal projections. We thank P. Wang and C. Jiang for surgical assistance.

AUTHOR CONTRIBUTIONS

M.H.M. and T.H.M. designed the study. M.H.M., A.W.C., D.A.M. and J.L. performed the experiments. M.H.M., A.W.C., M.M., J.L., Y.T.W. and M.R. analyzed the data. M.H.M., R.L., J.L. and J.D.B. participated in processing the Allen Mouse Brain Connectivity data. M.H.M., A.W.C. and T.H.M. wrote the manuscript, which all authors commented on and edited. T.H.M. supervised the study.

COMPETING FINANCIAL INTERESTS

The authors declare no competing financial interests.

1. Zhang, D. & Raichle, M.E. Disease and the brain's dark energy. *Nat. Rev. Neurol.* **6**, 15–28 (2010).
2. Destexhe, A. & Contreras, D. Neuronal computations with stochastic network states. *Science* **314**, 85–90 (2006).
3. Harris, K.D. & Thiele, A. Cortical state and attention. *Nat. Rev. Neurosci.* **12**, 509–523 (2011).
4. Arieli, A., Sterkin, A., Grinvald, A. & Aertsen, A. Dynamics of ongoing activity: explanation of the large variability in evoked cortical responses. *Science* **273**, 1868–1871 (1996).
5. Kenet, T., Bibitchkov, D., Tsodyks, M., Grinvald, A. & Arieli, A. Spontaneously emerging cortical representations of visual attributes. *Nature* **425**, 954–956 (2003).
6. Ferezou, I. *et al.* Spatiotemporal dynamics of cortical sensorimotor integration in behaving mice. *Neuron* **56**, 907–923 (2007).
7. Waters, J. & Helmchen, F. Background synaptic activity is sparse in neocortex. *J. Neurosci.* **26**, 8267–8277 (2006).
8. Luczak, A., Bartho, P. & Harris, K.D. Spontaneous events outline the realm of possible sensory responses in neocortical populations. *Neuron* **62**, 413–425 (2009).
9. Han, F., Caporale, N. & Dan, Y. Reverberation of recent visual experience in spontaneous cortical waves. *Neuron* **60**, 321–327 (2008).
10. Vincent, J.L. *et al.* Intrinsic functional architecture in the anaesthetized monkey brain. *Nature* **447**, 83–86 (2007).
11. Leopold, D.A., Murayama, Y. & Logothetis, N.K. Very slow activity fluctuations in monkey visual cortex: implications for functional brain imaging. *Cereb. Cortex* **13**, 422–433 (2003).
12. Lu, H. *et al.* Rat brains also have a default mode network. *Proc. Natl. Acad. Sci. USA* **109**, 3979–3984 (2012).
13. de Pasquale, F. *et al.* A cortical core for dynamic integration of functional networks in the resting human brain. *Neuron* **74**, 753–764 (2012).
14. Hipp, J.F., Hawellek, D.J., Corbetta, M., Siegel, M. & Engel, A.K. Large-scale cortical correlation structure of spontaneous oscillatory activity. *Nat. Neurosci.* **15**, 884–890 (2012).
15. Wedeen, V.J. *et al.* Diffusion spectrum magnetic resonance imaging (DSI) tractography of crossing fibers. *Neuroimage* **41**, 1267–1277 (2008).
16. Frostig, R.D., Xiong, Y., Chen-Bee, C.H., Kvasnak, E. & Stehberg, J. Large-scale organization of rat sensorimotor cortex based on a motif of large activation spreads. *J. Neurosci.* **28**, 13274–13284 (2008).
17. White, B.R. *et al.* Imaging of functional connectivity in the mouse brain. *PLoS ONE* **6**, e16322 (2011).
18. Grinvald, A. & Hildesheim, R. VSDI: a new era in functional imaging of cortical dynamics. *Nat. Rev. Neurosci.* **5**, 874–885 (2004).
19. Mohajerani, M.H., McVea, D.A., Fingas, M. & Murphy, T.H. Mirrored bilateral slow-wave cortical activity within local circuits revealed by fast bihemispheric voltage-sensitive dye imaging in anesthetized and awake mice. *J. Neurosci.* **30**, 3745–3751 (2010).
20. Allen Institute for Brain Science. Allen Mouse Brain Connectivity Atlas. *Allen Brain Atlas Data Portal* ⟨http://connectivity.brain-map.org/⟩ (2012).
21. Kleinfeld, D. & Delaney, K.R. Distributed representation of vibrissa movement in the upper layers of somatosensory cortex revealed with voltage-sensitive dyes. *J. Comp. Neurol.* **375**, 89–108 (1996).
22. Lim, D.H. *et al. In vivo* large-scale cortical mapping using channelrhodopsin-2 stimulation in transgenic mice reveals asymmetric and reciprocal relationships between cortical areas. *Front. Neural Circuits* **6**, 11 (2012).
23. Mao, T. *et al.* Long-range neuronal circuits underlying the interaction between sensory and motor cortex. *Neuron* **72**, 111–123 (2011).
24. Grandy, T.H., Greenfield, S.A. & Devonshire, I.M. An evaluation of *in vivo* voltage-sensitive dyes: pharmacological side effects and signal-to-noise ratios after effective removal of brain-pulsation artifacts. *J. Neurophysiol.* **108**, 2931–2945 (2012).
25. Akemann, W. *et al.* Imaging neural circuit dynamics with a voltage-sensitive fluorescent protein. *J. Neurophysiol.* **108**, 2323–2337 (2012).
26. Liu, C. *Beyond Pixels: Exploring New Representations and Applications for Motion Analysis*. PhD thesis, Massachusetts Institute of Technology (2009).
27. Takagaki, K., Zhang, C., Wu, J.Y. & Ohl, F.W. Flow detection of propagating waves with temporospatial correlation of activity. *J. Neurosci. Methods* **200**, 207–218 (2011).
28. Bullmore, E. & Sporns, O. Complex brain networks: graph theoretical analysis of structural and functional systems. *Nat. Rev. Neurosci.* **10**, 186–198 (2009).
29. Poulet, J.F. & Petersen, C.C. Internal brain state regulates membrane potential synchrony in barrel cortex of behaving mice. *Nature* **454**, 881–885 (2008).
30. Haider, B., Hausser, M. & Carandini, M. Inhibition dominates sensory responses in the awake cortex. *Nature* **493**, 97–100 (2013).
31. Polack, P.O. & Contreras, D. Long-range parallel processing and local recurrent activity in the visual cortex of the mouse. *J. Neurosci.* **32**, 11120–11131 (2012).
32. Huang, X. *et al.* Spiral wave dynamics in neocortex. *Neuron* **68**, 978–990 (2010).
33. Sato, T.K., Nauhaus, I. & Carandini, M. Traveling waves in visual cortex. *Neuron* **75**, 218–229 (2012).
34. Niell, C.M. & Stryker, M.P. Modulation of visual responses by behavioral state in mouse visual cortex. *Neuron* **65**, 472–479 (2010).
35. Wilson, M.A. & McNaughton, B.L. Reactivation of hippocampal ensemble memories during sleep. *Science* **265**, 676–679 (1994).
36. Euston, D.R., Tatsuno, M. & McNaughton, B.L. Fast-forward playback of recent memory sequences in prefrontal cortex during sleep. *Science* **318**, 1147–1150 (2007).
37. Douglas, R.J. & Martin, K.A. Mapping the matrix: the ways of neocortex. *Neuron* **56**, 226–238 (2007).
38. Reid, R.C. From functional architecture to functional connectomics. *Neuron* **75**, 209–217 (2012).
39. Shmuel, A. & Leopold, D.A. Neuronal correlates of spontaneous fluctuations in fMRI signals in monkey visual cortex: implications for functional connectivity at rest. *Hum. Brain Mapp.* **29**, 751–761 (2008).
40. Grienberger, C. *et al.* Sound-evoked network calcium transients in mouse auditory cortex *in vivo*. *J. Physiol.* (*Lond.*) **590**, 899–918 (2012).
41. Buzsaki, G. *et al.* Nucleus basalis and thalamic control of neocortical activity in the freely moving rat. *J. Neurosci.* **8**, 4007–4026 (1988).
42. Beier, K.T. *et al.* Anterograde or retrograde transsynaptic labeling of CNS neurons with vesicular stomatitis virus vectors. *Proc. Natl. Acad. Sci. USA* **108**, 15414–15419 (2011).
43. Osakada, F. *et al.* New rabies virus variants for monitoring and manipulating activity and gene expression in defined neural circuits. *Neuron* **71**, 617–631 (2011).
44. Cardin, J.A. *et al.* Driving fast-spiking cells induces gamma rhythm and controls sensory responses. *Nature* **459**, 663–667 (2009).
45. Tamamaki, N. & Tomioka, R. Long-range GABAergic connections distributed throughout the neocortex and their possible function. *Front. Neurosci.* **4**, 202 (2010).
46. Alivisatos, A.P. *et al.* The brain activity map project and the challenge of functional connectomics. *Neuron* **74**, 970–974 (2012).
47. Bohland, J.W. *et al.* A proposal for a coordinated effort for the determination of brainwide neuroanatomical connectivity in model organisms at a mesoscopic scale. *PLoS Comput. Biol.* **5**, e1000334 (2009).
48. Li, A. *et al.* Micro-optical sectioning tomography to obtain a high-resolution atlas of the mouse brain. *Science* **330**, 1404–1408 (2010).
49. Kleinfeld, D. *et al.* Large-scale automated histology in the pursuit of connectomes. *J. Neurosci.* **31**, 16125–16138 (2011).
50. Azin, M., Guggenmos, D.J., Barbay, S., Nudo, R.J. & Mohseni, P. A miniaturized system for spike-triggered intracortical microstimulation in an ambulatory rat. *IEEE Trans. Biomed. Eng.* **58**, 2589–2597 (2011).

ONLINE METHODS

Animals. Adult (~25 g) male C57BL/6J mice were used ($n = 30$) for most experiments, and adult male (~25 g) ($n = 7$) ChR2 transgenic mice (line 18, stock 007612, strain B6.Cg-Tg (Thy1-COP4/EYFP) 18Gfng/J; the Jackson Laboratory) were used for a subset of these experiments. Mice were housed in clear plastic cages in groups of two to five under a 12 h light, 12 h dark cycle. Mice were given *ad libitum* access to water and standard laboratory mouse diet at all times. Mice used in the awake imaging experiments were housed singly after head-restraint implantation surgery. The animal protocols were approved by the University of British Columbia Animal Care Committee and were in accordance with guidelines set forth by the Canadian Council for Animal Care.

Surgery. At approximately 16 weeks of age, mice were given a craniotomy. Mice were anesthetized with isoflurane (1.0–1.5%) for induction and during surgery, and a reduced maintenance concentration of isoflurane (0.5%) was used later during data collection. Mice were placed on a metal plate that could be mounted onto the stage of the upright macroscope, and the skull was fastened to a steel plate. A 7 × 6 mm unilateral craniotomy (bregma 2.5 to −4.5 mm, lateral 0 to 6 mm) was made, and the underlying dura was removed, as described previously[19]. Throughout surgery and imaging, body temperature was maintained at 37 °C using a heating pad with a feedback thermistor. In some cases, mice were also given a tracheotomy to assist with breathing.

VSD imaging. For *in vivo* VSD imaging, the dye RH-1692 (Optical Imaging, New York, NY)[51] was dissolved in 4-(2-hydroxyethyl)-1-piperazineethanesulfonic acid (HEPES)-buffered saline solution (1 mg ml^{-1}) and applied to the exposed cortex for 60–90 min, which stained all neocortical layers, as reported previously[19]. VSD imaging began ~30 min after washing unbound VSD. To minimize movement artifacts due to respiration, the brain was covered with 1.5% agarose made in HEPES-buffered saline and sealed with a glass coverslip. For VSD data collection, 12-bit images were captured with either 5- or 6.67-ms temporal resolution with a charge-coupled device (CCD) camera (1M60 Pantera, Dalsa, Waterloo, ON) and an EPIX E4DB frame grabber with XCAP 3.1 imaging software (EPIX, Inc., Buffalo Grove, IL). VSD was excited with a red LED (Luxeon K2, 627-nm center) and excitation filters of 630 ± 15 nm as described[19]. Images were taken through a macroscope composed of front-to-front video lenses (8.6 × 8.6 mm field of view, 67 μm per pixel). The depth of field of our imaging setup was 1 mm (ref. 22). VSD fluorescence was filtered using a 673- to 703-nm bandpass optical filter (Semrock, New York, NY). Because animal brain states show spontaneous change[19], we averaged 10–45 trials of stimulus presentation to reduce these effects. To correct for time-dependent changes in VSD signals that accompany all imaging, we also collected a number of nonstimulation trials that were used for normalization of the stimulated data. A 10-s interval between each sensory stimulation was used. To reduce potential VSD signal distortion caused by the presence of large cortical blood vessels, we focused into the cortex to a depth of ~1 mm. In our previous work, we measured VSD fluorescence across the cortex using histology and demonstrated relatively high labeling at a depth of ~750 μm (ref. 19). Nonetheless, to reduce regional bias in VSD signal caused by uneven dye loading or brain curvature, all VSD responses were expressed as a percentage change relative to baseline VSD responses ($\Delta F/F_0 \times 100\%$) using Matlab (Mathworks, Natick, MA). VSD imaging of spontaneous activity was performed in the absence of visual, olfactory, tactile or auditory stimulation during 30-s periods with 6.67-ms (150 Hz) temporal resolution. Slow, time-dependent reductions in VSD fluorescence were corrected in Matlab using a zero-phase lag Chebyshev bandpass filter (zero-phase filter) at 0.1–6 Hz. Ambient light resulting from VSD excitation (630 nm) was measured at 8.65×10^{-3} W m^{-2}. The total duration of the VSD excitation in a typical imaging experiment ranged from 900 to 1,200 s. VSD $\Delta F/F_0$ (%) and cortical EEG power were stable during recordings of up to 25 min (**Supplementary Fig. 2c**,**d**), indicating little phototoxicity under the conditions we used. The fluorescence changes were quantified as $(F - F_0)/F_0 \times 100$, where F is the fluorescence signal at any given time and F_0 is the average of fluorescence over all frames.

VSD imaging in awake mice. Young (8–10 weeks old) male C57BL/6 mice ($n = 6$) were surgically implanted with a plastic screw[19] on the skull for immobilization by connecting to a fixed connector. After 7 d of recovery, mice were habituated to head restraint, as described previously[19], and situated on top of a running wheel. Once the mice were habituated, a 7 × 6 mm craniotomy was performed under isoflurane anesthesia (0.5–2% maintenance mixed with oxygen) and then the mice were transferred to an awake imaging setup in which they were head restrained in a relaxed posture. To wake the mice, the isoflurane and oxygen were stopped and the anesthesia mask was removed. VSD imaging data were obtained over the next 1–2 h. The body temperature of the mice was maintained with a heat lamp. Awake VSD imaging of spontaneous activity imaging was performed in the absence of visual and auditory stimulation during 30-s periods. The 627-nm LED light used for VSD excitation or the infrared light used for behavioral observation did not result in a visual response. The use of a behavioral monitoring camera confirmed that the mice were indeed awake and relatively unstressed, as grooming, whisking, walking and running were observed. After image acquisition in the awake state, mice were anesthetized with isoflurane, and spontaneous and sensory-evoked activity were recorded in the lightly anesthetized state. An analgesic, buprenorphine, was injected (0.075 mg per kg body weight intraperitoneally) 24 h before awake VSD recordings. We used a second Dalsa 1M60 camera (150 Hz) to capture body and whisker movements under infrared illumination.

Cortical EEG recordings. A Teflon-coated, chlorided silver wire (0.125 mm) was placed on the right edge of the craniotomy. A reference electrode was placed on the nasal bone. The cortical signal was amplified (× 1,000) and filtered (0.1–1,000 Hz) using an A-M Systems (Sequim, WA) Model 1700 AC amplifier.

LFP recordings. A silicon multielectrode (NeuroNexus Technologies) was used for recording LFP. The was LFP signal was amplified (× 1,000) and filtered (0.1–1,000 Hz) using a 16-channel data acquisition system (USB-ME16-FAI-System, Multi Channel Systems).

EMG recording. A Teflon-coated, chlorided silver wire (0.125 mm) was fixed using conductive glue to a thin acupuncture needle (0.14 mm) and inserted into the neck muscles. A reference electrode was placed on the back of the mouse under the skin. The EMG signal was amplified (× 1,000) and filtered (1–1,000 Hz) using an A-M Systems (Sequim, WA) Model 1700 AC amplifier.

Sensory stimulation. Sensory stimuli were used to generate maps of the sensory cortical areas of (in no particular order) forelimb, hindlimb, whisker, visual and auditory stimulation. To stimulate the forelimbs and hindlimbs, thin acupuncture needles (0.14 mm) were inserted into the paws, and a 0.2–1 mA, 1-ms electrical pulse was delivered. To stimulate a single whisker (C2), the whisker was attached to a piezoelectric device (Q220-A4-203YB, Piezo Systems, Inc., Woburn, MA) and given a single 1-ms tap using a square pulse. The whisker was moved at most 90 μm in an anterior-to-posterior direction, which corresponds to a 2.6° angle of deflection. A 1-ms pulse of combined green and blue light was delivered as visual stimulation. A single 1-ms tone (25 kHz) was used as auditory stimulation. Averages of sensory stimulation were calculated from 10–40 trials of stimulation with an interstimulus interval of 10 s.

Photostimulation. A diode-pumped solid-state laser emitting 473-nm light (CNI Optoelectronics, Changchun, China) was used to stimulate ChR2-expressing neurons. The beam was positioned on the cortex using custom software written in IGOR PRO (Portland, OR), which controlled galvanometer scan mirrors (Cambridge Tech, Lexington, MA) through analog output voltage from a PCI-6110 DAQ instrument (National Instruments, Austin, TX), as reported previously[22]. The beam diameter measured through the objective was 70 μm and the beam was nearly collimated. The IGOR program controlled the overall timing of individual stimulation trials with TTL triggers to XCAP software. Low-amplitude and short-duration single laser pulses were used to ensure sufficient activation and a low laser-stimulus artifact (2.5–5 mW, 1-ms pulse). Consistent with previous data, this brief activation led to EEG depolarization[22]. Nineteen ROIs were selected for photostimulation. All regions were targeted for semirandom photostimulation for a total of 19 stimulation sites in one hemisphere. Each site was stimulated 5–10 times (10-s interstimulus interval), and replicate responses were averaged together[22].

Data analyses. For region-based correlation analyses (**Supplementary Fig. 4**), 18 5 × 5 pixel ROIs were selected. Sensory stimulation was used to determine the coordinates for the primary sensory areas (HLS1, FLS1, BCS1, V1 and A1),

doi:10.1038/nn.3499

secondary somatosensory areas (HLS2, FLS2 and BCS2) and M1 for the whiskers. From these primary sensory coordinates, the relative locations of additional associational areas were estimated using stereotaxic coordinates[52] (ptA, RS, M2, V2M (medial secondary visual cortex), V2L (lateral secondary visual cortex), mHL (hindlimb motor cortex) and mFL (forelimb motor cortex)).

To calculate the similarity between the spontaneous and cortical responses to different forms of sensory stimulation, we first created templates of different forms of sensory activity by taking the initial segment of the VSD-evoked responses (**Fig. 6a**). Then we calculated the correlation coefficient (correlation index) between the templates and each individual frame of spontaneous activity. Frames of spontaneous activity with a correlation coefficient greater than a given threshold were considered to be a 'match' to the evoked templates. To determine the threshold value, we calculated the maximum of the correlation coefficients between all sensory templates (hindlimb, forelimb, visual, auditory and whisker), and the results were multiplied by a constant factor (1.34). To find this constant factor, we measured the percentage of matched hindlimb templates as a function of a different constant factor for seven experiments (**Supplementary Fig. 6a**). The resulting plot (black) was fitted with an exponential curve (red). We chose the curve decay constant (blue dash line) as a constant factor (e^{-1}). For the multiple-frame template search, the first three frames after the initial activation of the sensory cortex were used (**Fig. 6a**,**d**). To create seed-pixel correlation maps (**Figs. 3**, **5**, **7** and **8** and **Supplementary Figs. 3**, **5** and **7**), we calculated the zero-lag Pearson product-moment correlation between the VSD signal time course extracted from a seed pixel of interest and every pixel within the imaging area. The lengths of activity used to calculate the correlation index were 300 s for spontaneous activity and 510 ms for sensory-evoked and photostimulation-evoked responses.

Optical flow analysis. Optical flow approaches calculate vector fields that determine the apparent velocities of objects in time-varying image sequences[26]. We used a combined local-global algorithm developed using a Matlab toolbox to quantify the trajectory of the maximum velocity position at various time points after sensory- or photostimulation-evoked VSD activity. A detailed description of the combined local-global algorithm has been documented previously[26]. The Matlab toolbox is available for download (http://people.csail.mit.edu/celiu/OpticalFlow/). We used the Mathematica software (Wolfram Research, IL) built-in 'ListStreamPlot' function to calculate streamlines, which uses a high-order Runge-Kutta method. We used this analysis to identify sink and source locations on the cortex. We calculated the outgoing or ingoing flow in small closed regions, which can be performed by numerical realization of divergence operator ($\nabla \times \boldsymbol{V}$), where $\boldsymbol{V}$ is the velocity vector. Using this approach, regions with highly positive or negative total flow can be recognized as sources or sinks of the vector field. Pre-smoothing iterations to find the singularities of the velocity vector fields were performed before numerical flow calculations.

Pharmacology. For pharmacological experiments, the cortex was covered with HEPES-buffered saline solution to allow for later topical application of 30 μM TTX. The cortex was incubated with TTX for 30 min before further imaging.

Statistics. For the composite data shown in **Figures 4** and **8** and **Supplementary Figures 2**, **3**, **5** and **6**, we used one-way ANOVA and a Bonferroni *post-hoc* analysis. For the composite data in **Supplementary Figures 1** and **4**, we used two-way ANOVA and a Bonferroni *post-hoc* analysis. For the composite data in **Figure 2**, we used the following test: first, we determined the locations of maximal activation for each mouse independently. Then we computed the (vector) mean and variance of the maximal activation across mice. Then we subtracted each of the two coordinates from the mean for each pair of sensory modalities and divided by the squared s.e.m.:

$$F_{i,j,k,t} = \frac{(\bar{x}_k^i - \bar{x}_k^j)^2}{\frac{(s_k^i)^2}{n} + \frac{(s_k^j)^2}{n}}$$

where i and j index the sensory modality, $k = 1, 2$ indexes the coordinate (horizontal or vertical), t indexes the time step, and n is the number of mice used (usually seven). Under the null hypothesis, these ratios would have an $F(1, n-1)$ distribution. We then computed the sum of these F scores over coordinates k and time steps t (five steps):

$$F^*_{i,j,k} = \sum_{t=1}^{5} F_{i,j,k,t}$$

There is no analytic expression for the distribution of a sum of independent F scores. We therefore simulated the distribution of such scores by generating independent draws from $F(1,6)$ distributions and adding them in groups of five to obtain a distribution of F^* under the null hypothesis of no difference in trajectories. We did 10,000 draws and set our threshold at $P < 0.001$, which was the largest score from this simulation. We followed the same strategy for showing that there was no significant difference in the sink of each sensory modality, except that there was no dependence on t.

There are several places in which correlations are used in this paper to make comparisons within and across mice. In **Figures 3** and **5** and **Supplementary Figure 5** (and the group analyses in **Supplementary Figs. 3** and **5**), we computed seed-pixel correlation maps using temporal correlation of data obtained from different origins of activity (spontaneous, sensory evoked or photostimulation evoked) for multiple cortical regions for each mouse. We then compared the sets of these seed-pixel correlation maps using spatial correlation analysis within the mice (examining how relative patterns change within a subject), which removes the necessity of registration and alignment across mice. 'Sets' were defined in this context as seed-pixel correlation maps generated from the same seed-pixel location (for example, HLS1) and by the origin of the activity from which the maps were generated (spontaneous, sensory evoked or photostimulation evoked) for each mouse. From this information, we drew the conclusion that some sets are relatively homogeneous (by the same seed-pixel location but obtained from different origins of activity, for example, sHLS1, eHLS1 or photostimulation-evoked HLS1 (pHLS1) compared with each other; **Fig. 3** and **Supplementary Fig. 3**) and distinct from other sets (by different seed-pixel locations but obtained from the same or different origins of activity, for example, sHLS1, eFLS1 or pFLS1; **Supplementary Figs. 3** and **5**). In this case, the statistical significance of these comparisons depended on how consistent the individual spatial correlations were within a set (composed of up to nine mice) and how different they were between sets. To determine statistical significance across mice, we calculated t statistics for each comparison of one set of seed-pixel correlation maps with another set of seed-pixel correlation maps, computed using spatial correlation analysis in an identical fashion from different data (different sets across mice). For these analyses, the degrees of freedom were constrained by the number of experimental replicates (number of mice) used for the comparisons under the same experimental conditions.

To minimize the local contribution of correlation values around the seed pixel in the spatial correlation analyses, we used a two-dimensional Gaussian fit to create a template image for each individual correlation map that models the local distribution of the correlation values centered around the seed pixel. To exclude the contribution of the first-order local correlations, we subtracted the template image from its corresponding original map. The resulting residual map contained only the second-order long-range correlation. The exclusion zone often encompassed several millimeters (**Supplementary Fig. 3a**). We used these residual maps in our group data correlation analysis between maps obtained from sensory-evoked, spontaneous and optogenetically evoked activity (**Supplementary Fig. 3b**,**c**), as well as in our structure analysis (**Fig. 8**).

As an alternative method to the comparison of correlation image sets described above (**Supplementary Fig. 3** as an example), we also used an ROI-based comparison of the correlation index at regions identified using the combination of sensation-derived and AMBC Atlas–derived functional areas (**Supplementary Fig. 4**). To measure the amount of variance of spontaneous activity that can be accounted for by sensory motifs, we computed the mean variance (r^2) over the whole time series of spontaneous activity (215.74 s, 0.1–6.0 Hz bandpass filtered) for each mouse.

No statistical methods were used to predetermine sample sizes, but our sample sizes are similar to those reported in previous publications[19]. Data collection and analyses were not performed blind to the conditions of the experiment. However, experimental mice belonged largely to a single group, and quantitative automated methods were used to minimize experimenter bias. No method

of randomization was used to assign mice to experimental groups. The data distribution was assumed to be normal, but this was not formally tested. Error bars and ± ranges represent the s.e.m. $^{*}P < 0.05$, $^{**}P < 0.01$, $^{***}P < 0.001$. All the statistical tests were two sided.

Two-dimensional reconstruction of axonal projection maps. Images of 100-μm coronal sections of mice injected with GFP-expressing AAV were downloaded from the Allen Institute for Brain Science (http://connectivity.brain-map.org/) at a resolution of 2.8 μm per pixel. For each mouse, a complete series of images through the entire neocortex was assembled into a three-dimensional stack. Minor rotations and translations were applied to each image in the stack to correct slight misalignments, and the stack was cropped to include only the injected hemisphere and rotated laterally 30° to match the angle of the mouse head in the VSD experiments. Structural data outside of the cortex were masked to remove contributions from subcortical labeling, and an average intensity projection was made through the stack. To register the anatomical maps obtained from different mice, three anatomical markers of the brain were used: midline, the position of the most posterior segment of the dentate gyrus and the position of the most anterior portion of the lateral ventricle of the injected hemisphere (right hemisphere). Because these last two positions were located within the subcortical regions of the brain, we made an orthographic projection of these positions along the vertical direction in the rotated images of the cortex.

Registration of functional and anatomical maps. Functional and anatomical maps were aligned using a combination of anatomical landmarks and experimentally determined functional brain areas. Briefly, in each mouse, we used the position of the center of V1 sensory cortex, determined by VSD imaging, and the location of the bregma, measured from the skull, to register the images with structural connectivity maps from the Allen Institute. Equivalent landmark positions from the structural data, V1 and bregma were extrapolated from measurements of the position of the most posterior segment of the dentate gyrus and the most anterior portion of the lateral ventricle.

51. Shoham, D. *et al.* Imaging cortical dynamics at high spatial and temporal resolution with novel blue voltage-sensitive dyes. *Neuron* **24**, 791–802 (1999).
52. Paxinos, G. & Franklin, K.B.J. *The Mouse Brain in Stereotaxic Coordinates* (Elsevier Academic Press, Amsterdam, Boston, 2004).

doi:10.1038/nn.3499